Reaction cross sections for protons on ^{12}C, ^{40}Ca, ^{90}Zr, and ^{208}Pb at energies between 80 and 180 MeV

A. Auce, A. Ingemarsson, R. Johansson, M. Lantz, and G. Tibell
Department of Radiation Sciences, Uppsala University, Box 535, S-75181 Uppsala, Sweden

R. F. Carlson and M. J. Shachno
Department of Physics, University of Redlands, Redlands, California 92373, USA

A. A. Cowley, G. C. Hillhouse, N. M. Jacobs, J. A. Stander, and J. J. van Zyl
Department of Physics, University of Stellenbosch, Private Bag X1, Matieland 7602, South Africa

S. V. Förtsch, J. J. Lawrie, F. D. Smit, and G. F. Steyn
iThemba Laboratory for Accelerator-based Sciences, Faure, South Africa
(Received 25 February 2005; published 28 June 2005)

Results of reaction cross-section measurements on ^{12}C, ^{40}Ca, ^{90}Zr, and ^{208}Pb at incident proton energies between 80 and 180 MeV and for ^{58}Ni at 81 MeV are presented. The experimental procedure is described, and the results are compared with earlier measurements and predictions using macroscopic and microscopic models.

DOI: 10.1103/PhysRevC.71.064606 PACS number(s): 25.40.−h, 24.10.Ht

I. INTRODUCTION

Experimental reaction cross sections of proton scattering from nuclei are of fundamental importance to our understanding of proton-induced reactions. These values find applications in chemistry, medicine, and astrophysics, and thus they constitute one of the motivations for the determination of global nucleon optical models. Such models can be used to predict elastic scattering and the reaction cross section at any energy. They can also generate distorted waves to be used in theories for predictions of other proton-induced reactions in the irradiated medium.

The global potentials are derived from the vast set of existing experimental data comprising angular distributions of differential cross sections, polarizations, asymmetries, and spin-rotation parameters. However, the derived potentials are not unique and manifest ambiguities; therefore, a knowledge of the value of the reaction cross section may provide some guidance. One reason why reaction cross sections in the past could often not be fully exploited as a powerful constraint in the derivation of the global potentials is that in many cases the existing data are much less accurate than the data for differential cross sections and other parameters. Furthermore, apart from the lack of reaction cross section data on some important target nuclei, existing experimental data often manifest serious inconsistencies.

We have measured proton reaction cross sections for ^{12}C, ^{40}Ca, ^{90}Zr, and ^{208}Pb in the energy range 80–180 MeV and for ^{58}Ni at 81 MeV. The measurements were performed with beams from the Separated Sector Cyclotron at iThemba LABS in South Africa. The data are compared with earlier measurements and theoretical predictions.

The preliminary results from these measurements were presented at the International Conference on Nuclear Data for Science and Technology, held in Santa Fe, New Mexico, in September 2004 [1].

II. EXPERIMENTAL METHOD

The experimental apparatus is a modified version of the one used for reaction cross-section measurements of ^{3}He and ^{4}He in the energy range 20–50 MeV/nucleon [2,3] and 65 MeV protons [4]. Some modifications to the equipment as described below were necessary to accommodate the higher proton energies.

A. Particle beams

The experiments were performed at the iThemba Laboratory for Accelerator-Based Sciences (Faure, South Africa) with proton beams from the iThemba Separated Sector Cyclotron. The extracted beams had a momentum resolution $\Delta p/p$ of 0.5% corresponding to an energy resolution of 0.8 MeV (full width at half maximum, FWHM) at 80 and 1.8 MeV at 180 MeV.

Because of the use of a CsI stopping detector, which has a slow signal compared with plastic scintillators, the experiment requires a beam with very low intensity, of the order of 10^3 particles per second. This level is obtained by reducing the intensity in the ion source in combination with several attenuating collimators along the beamline between the cyclotron and the experimental setup. In the case of the higher energies, the faint beam method as described in Ref. [5] was also used to reduce the beam intensity. Any combination of three different copper transmission meshes that accurately reduce the intensity by up to 10^6 can be inserted in the beam between the ion source and the injector cyclotron.

The experimental method is based on a modified transmission technique, where a proton beam is incident on a target and the outgoing particles are energy analyzed in order to separate transmitted and elastically scattered protons from reaction products. The basic principles of the measurements have been described in Ref. [6].

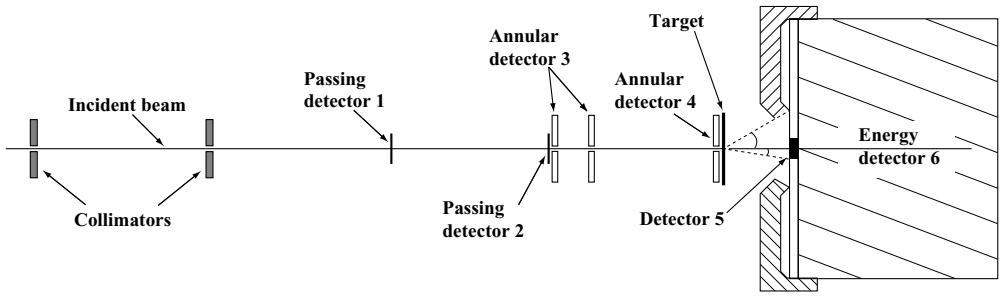

FIG. 1. Schematic overview of the apparatus.

False reaction events are eliminated by measuring the background in target-out measurements, and the reaction cross section is determined by the difference in the number of reaction events from target-in and target-out measurements.

The experimental arrangement is shown in Fig. 1. The two beam-defining brass collimators shown in Fig. 1 were chosen to be thick enough to stop 200 MeV protons. Incident protons are identified by plastic scintillators in a passing detector telescope, containing two passing detectors and two annular detectors. The passing detectors are used for the selection of protons with proper energy, while the annular detectors serve as active collimators, ensuring that the identified protons are correctly directed on the target.

The targets are mounted on a wheel which can be rotated to a selected position. One empty position on the wheel is used for target-out measurements. The targets, all significantly larger than the size of the beam, have thicknesses of the order of 100 mg/cm^2, giving beam energy losses of about 0.5 MeV and straggling effects of 0.3 MeV (FWHM) or less over the energy range 80–180 MeV.

Behind the target, the outgoing particles are energy analyzed in a CsI energy detector, thick enough to stop 200 MeV protons, in order to identify all unaffected or elastically scattered protons. The beam intensity is reduced with collimators to the order of 2000 protons per second. About 99.9% of the incident particles are unaffected by the target, and hence all enter the energy detector. The target thickness is very small in comparison to that of the energy detector; consequently, most of the particles detected with an energy below the elastic peak are those that have undergone reactions in the detector itself.

More than 98% of the nonreaction protons are concentrated in a narrow forward cone that covers less than 1% of the total solid angle. To reduce the statistical uncertainty, all particles that enter the forward cone are excluded from the analysis. Immediately in front of the energy detector is a small transmission detector (see Fig. 2) that consists of an array of three overlapping plastic scintillators, one circular and two ring shaped, which allows different solid angles to be covered simultaneously. Through this arrangement, five forward cones are defined, enabling measurements that range in steps between 99.0 and 99.8% of the total solid angle. The measured reaction cross section outside of an excluded forward cone is denoted as the partial reaction cross section.

During the experiment, data signals originating from the detectors are accumulated in an online data-acquisition computer system.

In the offline analysis, the signals from the transmission detector array and the CsI detector are sorted into regions and the number of reaction events is determined for each region. Typical energy spectra for each region with and without the target are shown in Fig. 3. The energy resolution is 1.5–3 MeV (FWHM). False reactions from the target-out measurements are subtracted from the number of reactions for each solid angle. Corrections are also performed for elastic scattering outside of the energy detector as well as for the reduction of the detector efficiency due to reactions occurring in the CsI scintillator.

After the corrections have been applied, the partial reaction cross sections for five solid angles are obtained, each excluding a forward cone determined by the regions in the scintillator array.

The contributions in the excluded forward cone were found to be considerably smaller than those for ^{3}He, ^{4}He [2,3], and deuterons [7]. Furthermore, the results gave no indication of a deviation from a linear dependence and, more surprisingly, the correction was more or less the same at the higher energies. Therefore, the reaction cross section for the full solid angle was obtained by fitting and extrapolating a line through the data points. Figure 4 shows a typical example of the behavior

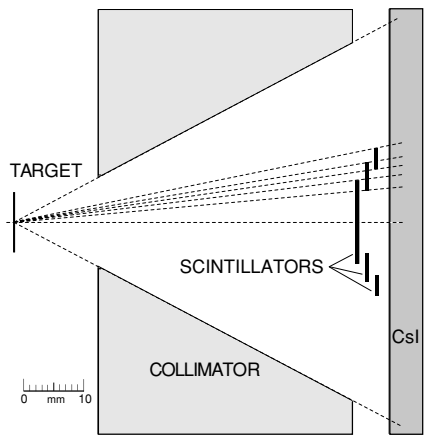

FIG. 2. Schematic overview of the transmission detector array of circular and ring shaped scintillators and the CsI energy detector after the target.

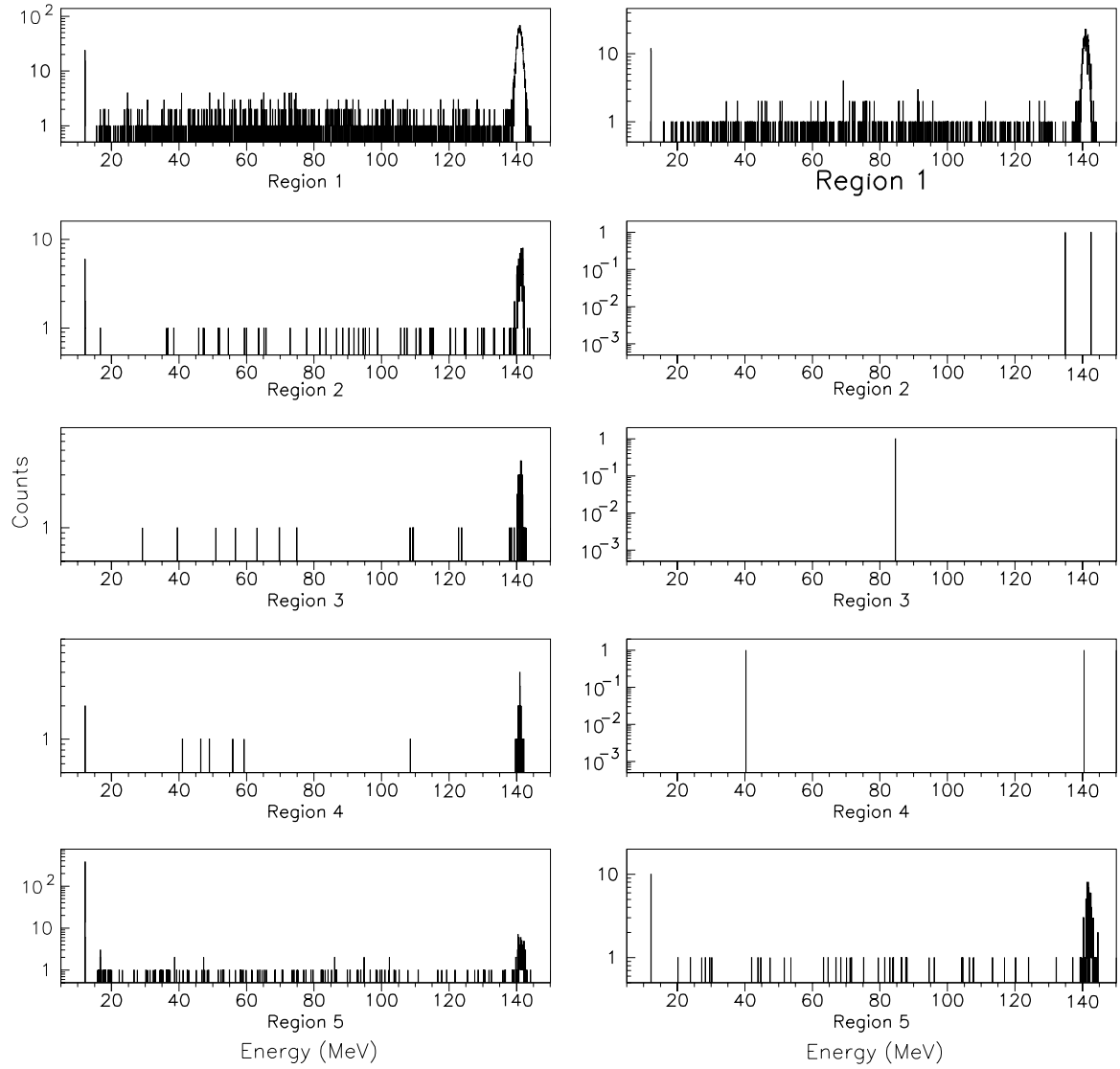

FIG. 3. Energy spectra obtained at 140 MeV with target ^{208}Pb (left) and without target (right).

of the partial reaction cross sections for 180 MeV protons on ^{12}C together with the extrapolated value. The uncertainty in the extrapolated value is obtained by the least-squares method.

III. RESULTS

Our experimental values are given in Table I and shown in Fig. 5 (closed circles) together with results from the compilation by Carlson [8] (open circles). The previous values obtained at 65 MeV [4] are also shown by closed circles. The errors shown are statistical. The systematic errors due to uncertainties in the thickness and the uniformity of the targets vary from 1–4% as given in Table II.

The experimental values are compared with the predictions of three different calculations which we have chosen because they have their origin from very different procedures. The theoretical results, which are shown as the curves in the figure, are predictions by using global potentials derived by Cooper *et al*. [9] and by Koning and Delaroche [10], as well as a prediction using a microscopic approach by Amos *et al*. [11]. As Klug *et al*. did in Ref. [12], we used the Koning and Delaroche global potential for ^{12}C in spite of the fact that in Ref. [10] they mention the mass range $24 \leqslant A \leqslant 209$. The general trend is that the predictions differ mainly in the slope of the energy dependence.

Cooper *et al*. derived global potentials in a relativistic approach using the Dirac equation and experimental results in the energy region 20–1040 MeV. The potentials are also available in a form that can be used in programs based on the non-relativistic Schrödinger equation. They provide four different potentials, and the results shown by the solid curves in Fig. 5 were obtained with the potentials denoted as EDAD (energy dependent and A dependent) fit 3 in [9].

Koning and Delaroche used experimental data in the energy region 1 keV to 200 MeV. The different parts of the optical potentials have a fixed geometry, with the same parameters for the real and imaginary central potentials. The fact that

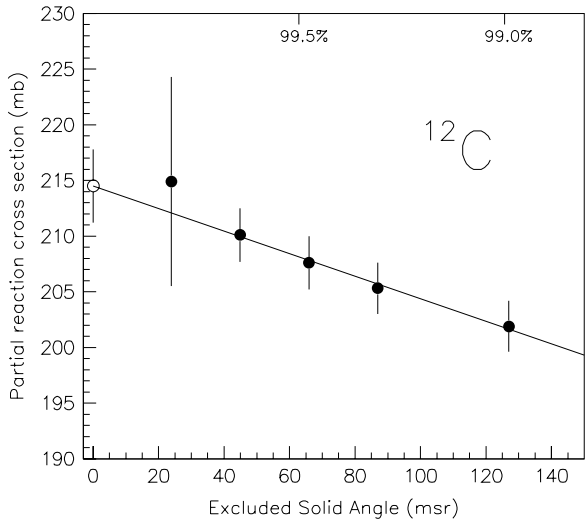

FIG. 4. Partial reaction cross sections obtained for 180 MeV protons on ^{12}C with different solid angles of the excluded forward cone. Solid line shows the best fit used for extrapolation to the full solid angle, assuming a linear dependence on the excluded solid angle. Open circle shows the extrapolated reaction cross section for the full solid angle.

the imaginary potentials have two components, one volume term and one surface peaked term, that vary independently, introduces an energy dependence in the shape of the imaginary potentials. The addition of the surface term also implies that the imaginary potential has a longer range than the real one. The results obtained with their global potential are shown in Fig. 5 as the dashed line.

Amos *et al*. performed microscopic calculations with nonlocal complex potentials obtained by folding an effective nucleon-nucleon interaction with matter densities from credible structure models of the target. These results are shown by the dotted curves.

TABLE I. Measured proton reaction cross sections in mb. Errors are statistical.

Energy	^{12}C	^{40}Ca	^{58}Ni	^{90}Zr	^{208}Pb
81	279 ± 10	660 ± 25	846 ± 34	1220 ± 60	2010 ± 80
100	275 ± 21	604 ± 24	–	1080 ± 60	1860 ± 90
119	237 ± 7	563 ± 12	–	1090 ± 50	1840 ± 60
141	222 ± 5	536 ± 8	–	997 ± 34	1780 ± 40
158	212 ± 4	524 ± 8	–	961 ± 27	1720 ± 40
180	211 ± 3	517 ± 7	–	934 ± 20	1720 ± 30

IV. DISCUSSION

A. General trends

Reference [13] showed that the energy dependence of the reaction cross sections for ^{3}He, ^{4}He, and ^{12}C could be

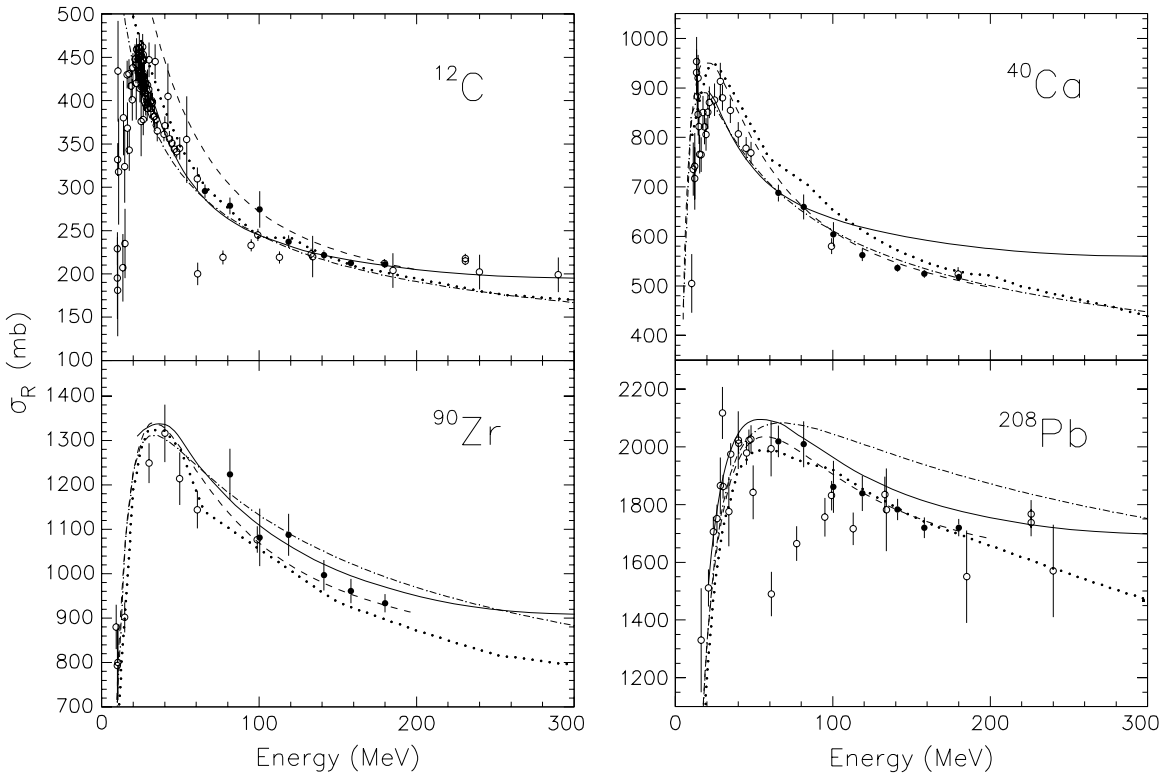

FIG. 5. Measured reaction cross sections (closed circles) compared with earlier data [8] (open circles), and theoretical predictions from global potential EDAD fit 3 by Cooper *et al*. [9] (solid curves), global potential by Koning and Delaroche [10] (dashed curves), and microscopic calculations by Amos *et al*. [11] (dotted curves). Dot-dashed curves are described in Sec. IV.

TABLE II. Target specifications.

Target	Enrichment	Thickness (mg/cm^2)	Thickness uncertainty (%)
^{12}C	Natural	78.9	1
^{40}Ca	Natural	138.1	2
^{58}Ni	99.79%	40.5	2
^{90}Zr	97.65%	77.5	2
^{208}Pb	88%	125.4	4

explained as an effect of the behavior of the matter densities at large radii and the variation in the nucleon-nucleon total cross section. The reaction cross sections shown in Fig. 5 also behave like the nucleon-nucleon total cross section with a minimum just above 200 MeV. As recently shown in [14], the approach of Ref. [13] can be used also for protons if the dependence of the matter densities becomes weaker for heavier targets.

The energy dependence of the reaction cross section in Fig. 5 was calculated from potentials that vary with energy. Note, however, that even if the potentials are fixed, the calculated reaction cross sections vary with energy. This is illustrated by the dot-dashed curves in Fig. 5, which were calculated from the optical potentials at 65 MeV using the global potentials of Cooper *et al*. [9]. These calculations reproduce the energy dependence rather well and also show that the energy-independent Coulomb potential causes the decrease at low energies. It should be noted, however, that an energy-independent potential will totally fail to reproduce the angular distributions.

The decrease in the reaction cross section with energy is best understood in the eikonal approach. This approach is quite accurate for protons, since noneikonal effects on the reaction cross sections for protons are rather small [15]. In the eikonal approach, the phase shift function for the impact parameter b, $\chi(b)$, is calculated from

$$\chi(b) = -\frac{1}{v_{\rm lab}} \int_{-\infty}^{\infty} U(b,z)dz, \tag{1}$$

where $U(b,z)$ is the optical potential and $v_{\rm lab}$ the velocity of the projectile in the laboratory system. The reaction cross section is then obtained from

$$\sigma_R = 2\pi \int_0^{\infty} b\,db(1 - e^{-2{\rm Im}[\chi(b)]}). \tag{2}$$

Thus the phase shift function and the absorption decrease with increasing energy for a fixed potential.

When comparing reaction cross-section data with predictions from optical model calculations, one must remember that the reaction cross section is only sensitive to the amplitude of the scattered waves and not to their phases. Therefore, the quality of a potential or a microscopic calculation must be judged by the quality of the fit to the reaction cross section as well as the quality of the angular distributions for all parameters in the elastic scattering.

B. Results for ^{12}C

Our new reaction cross-section data for ^{12}C show that some of the earlier measurements are clearly in error and should definitely be disregarded. The results for the angular distributions in the elastic scattering obtained at 65 and 200 MeV are shown in Fig. 6. These two energies, just below and above the energy region we have studied, were

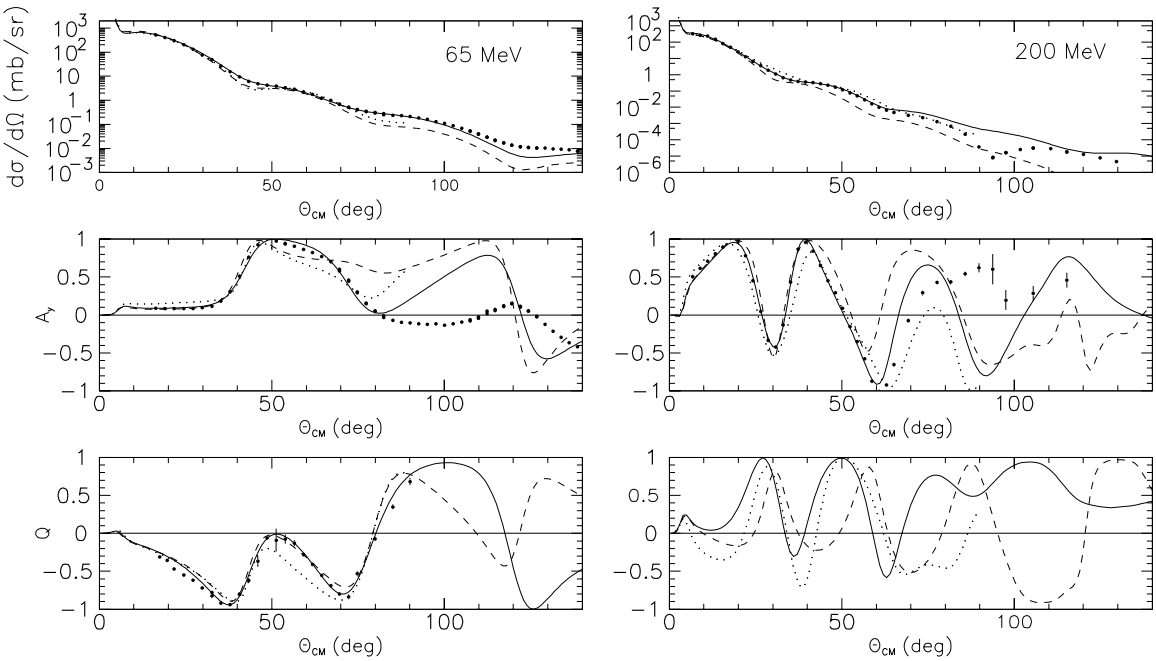

FIG. 6. Angular distributions of the differential cross section (top), asymmetry A_y (middle), and spin-rotation parameter Q (bottom) for the elastic scattering of 65 (left) and 200 MeV (right) protons from ^{12}C. See text and Fig. 5 caption for details of the theoretical calculations. Experimental results are from [16,17].

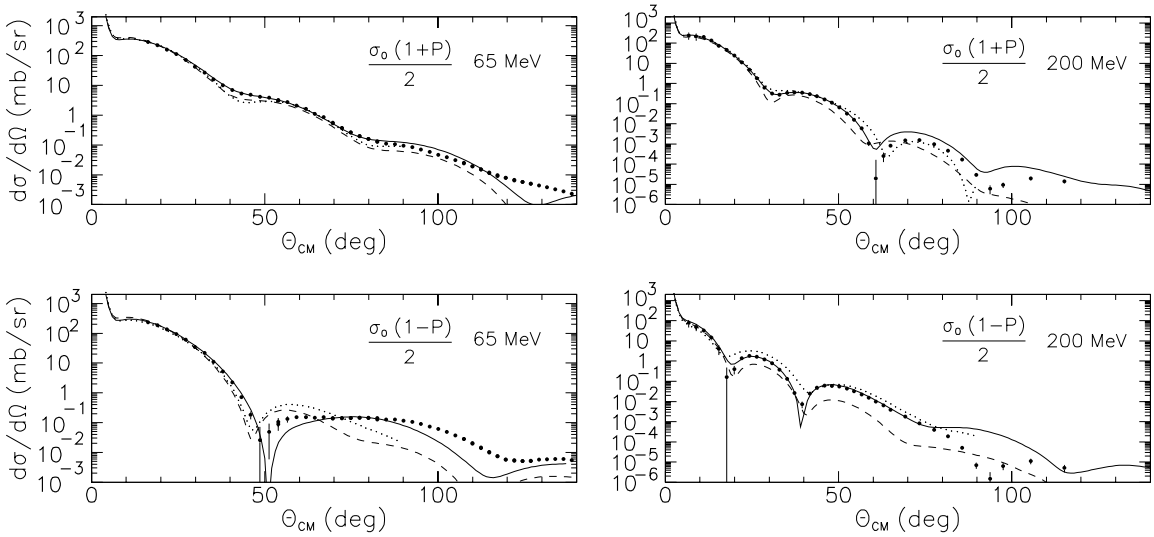

FIG. 7. Angular distributions for σ_+ and σ_- for the elastic scattering of 65 and 200 MeV protons from ^{12}C. See text and Fig. 5 caption for details of the theoretical calculations.

chosen because excellent data are available not only for the differential cross section and the asymmetry, but also for the spin rotation [16,17].

We should explain that we used the energy- and A-dependent potential EDAD3 for our calculations of the reaction cross section and the angular distributions for the prediction with the global potential of Cooper *et al*. The A-independent potential EDAI reproduces the angular distributions somewhat more accurately, but the prediction for the reaction cross section is less satisfactory; therefore, we preferred EDAD3 in this report. This fact illustrates the difficulties in deriving optical potentials and the importance of having data for both the angular distributions and the reaction cross section. Moreover, for most nuclei Koning and Delaroche provide an A-dependent as well as A-independent potential. We used the A-dependent potentials for all targets. Because one potential might be preferable at one energy but not at another energy, the results presented here should only be considered as illustrative examples.

Figure 6 shows that the three calculations all reproduce the angular distributions well for small angles. For larger angles, there are drastic differences in some cases. If the potentials are used for practical applications, however, they all predict the angular distributions and the reaction cross sections satisfactorily.

The quality of the angular distributions of the differential cross section and the asymmetry can also be investigated by calculating the differential cross section for protons with spin up and down in the scattering to positive angles. As discussed in Ref. [18], these differential cross sections are given by

$$\sigma_+ = \frac{\sigma_0(1+P)}{2}, \tag{3}$$

$$\sigma_- = \frac{\sigma_0(1-P)}{2}, \tag{4}$$

where σ_0 denotes the differential cross section for an unpolarized beam and P the polarization. The angular distributions for the polarization and the asymmetry oscillate around zero at both high and low energies. At intermediate energies and especially in the region 150–200 MeV, however, the polarization is predominantly positive and the maxima are often close to 1.0. Since $1 + P$ has its maximum values when $1 - P$ has its minimum values, the angular distributions will oscillate out of phase and the angular distributions for σ_- will show pronounced minima. The fact that σ_+ and σ_- are oscillating out of phase is, as discussed in Ref. [18], one reason why intermediate energy protons show less structure in the angular distributions for the differential cross sections than spinless projectiles. The results for σ_+ and σ_- obtained at 65 and 200 MeV are shown in Fig. 7. The predictions for σ_- are seen to differ much more from the experimental results than those for σ_+, which give the major contribution to the differential cross section.

Figure 8 shows the optical potentials obtained from Cooper *et al.* and from Koning and Delaroche. The microscopic calculations by Amos *et al.* do not automatically generate optical potentials and are not shown. The two global potentials will of course differ since they are generated by different approaches. The real potential, for example, is obtained from scalar and vector potentials with energy-dependent shapes and strengths in the approach by Cooper *et al*., whereas Koning and Delaroche use a Woods-Saxon form factor with fixed shape. Also, the Coulomb potentials differ; Koning and Delaroche use a uniform charge distribution, whereas Cooper *et al*. calculate the Coulomb potential from a realistic charge distribution. Substantial differences occur between the potentials obtained from the two approaches, but in the radial region 3–4 fm they are quite similar. The upper part of Fig. 8 shows the effective real central potential given by the sum of the real central potential and the Coulomb potential. The strength is considerably lower at the higher energy, and the shapes are drastically different at 200 MeV. Also, the other potentials in the two approaches, shown in the lower parts of Fig. 8, are similar in the region 3–4 fm, but differ for smaller radii.

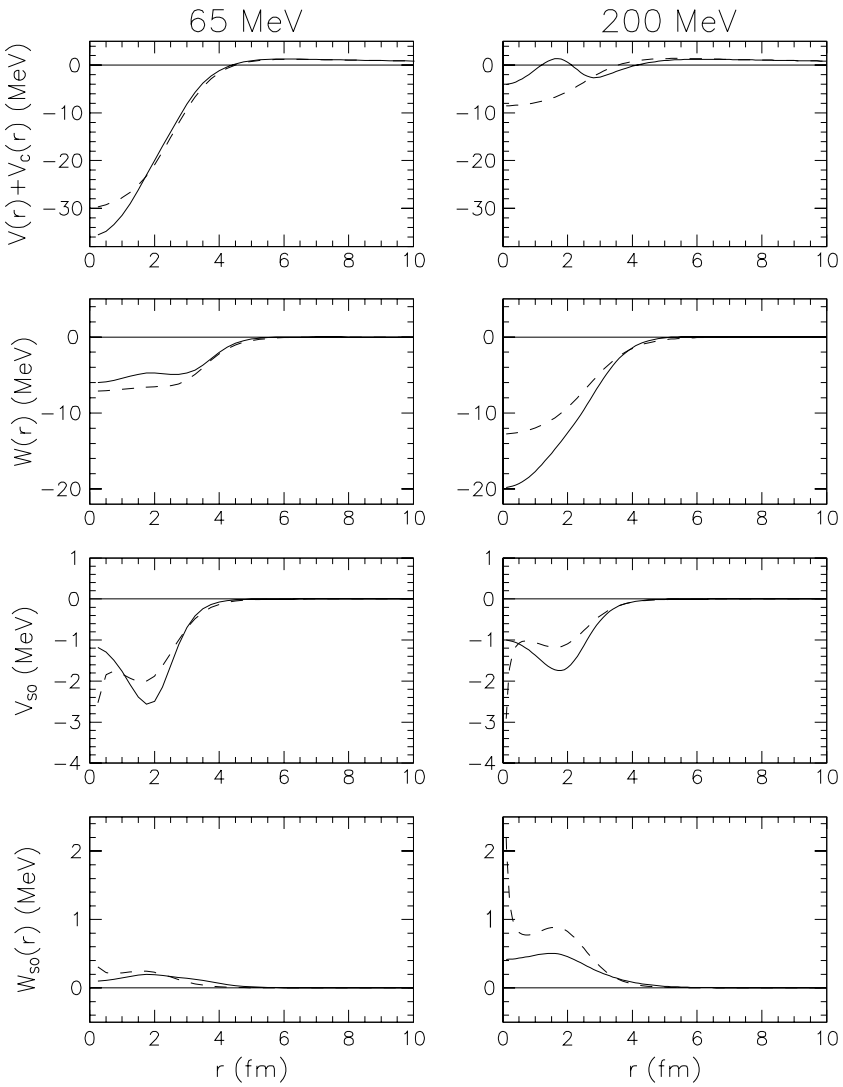

FIG. 8. Optical potentials for the elastic scattering of 65 and 200 MeV protons from ^{12}C. Solid curves, predictions by Cooper *et al*. [9]; dashed curves, predictions by Koning and Delaroche [10].

The phase shifts generated for the two global potentials will of course also differ. The reaction cross sections are given by the equation

$$\sigma_R = \frac{\pi}{k^2} \sum_{\ell} \left[(\ell + 1)\, T_{\ell}^{j=\ell+1/2} + \ell\, T_{\ell}^{j=\ell-1/2} \right], \qquad (5)$$

where the absorption coefficients T_{ℓ}^{j} are obtained from the S-matrix elements, S_{ℓ}^{j}, according to

$$T_{\ell}^{j} = 1 - \left| S_{\ell}^{j} \right|^2. \qquad (6)$$

Figure 9 shows absorption coefficients calculated with the potential by Cooper *et al*. and the potential by Koning and Delaroche. One can observe that the absorption coefficients differ appreciably for small ℓ values. Since the absorption coefficients are weighted by $\ell + 1$ and ℓ in Eq. (5), it is the absorption coefficients for large ℓ values that are most important for the reaction cross section. At 200 MeV, the results also differ for $j = \ell + 1/2$ for large ℓ values. Protons with spin down are much more strongly absorbed at 200 MeV. The large difference in absorption in the two channels also explains why the angular distributions for spin down have a diffractive structure, whereas protons with spin up have a refractive behavior.

Finally, it should be stressed that global potentials are not expected to reproduce the angular distributions as well as those optimized for one single energy. It turns out, however, that in proton scattering from ^{12}C extended to very large angles [19,20], the conventional parametrization of the optical potential must be modified to reproduce the large angle scattering. In Ref. [19], three different approaches were used to analyze the data up to 154°. The best fit to the differential cross-section data was obtained with a double Woods-Saxon shape for the real central potential (see Ref. [19]) and a semimicroscopic shape for the spin orbit potential. This approach gave not only the best fit to the angular distribution but also a better reproduction of the reaction cross sections. The fact that the reaction cross sections obtained in the three models differed in some cases by more than 30% emphasizes the need for reaction cross-section data in this type of investigation.

It is also interesting that when the range of data is extended to 180° [20] the optical model predictions overestimate the differential cross section by an order of magnitude.

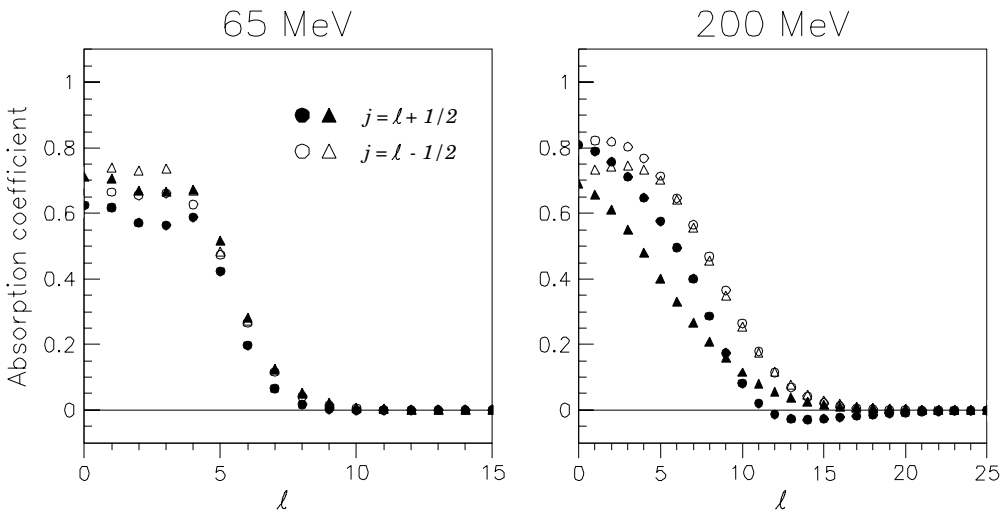

FIG. 9. Absorption coefficients in the scattering of 65 and 200 MeV protons from ^{12}C obtained from the global potential by Cooper *et al.* [9] (circles) and Koning and Delaroche [10] (triangles) for $j = \ell + 1/2$ (solid) and $j = \ell - 1/2$ (open).

C. Results for ^{40}Ca

The results for the reaction cross section for ^{40}Ca are in good agreement with the earlier measurements. The global potential by Cooper *et al.* underestimates the slope of the energy dependence over the whole energy region. The potential by Koning and Delaroche reproduces our data well, but overestimates the reaction cross sections below 80 MeV. The prediction by Amos *et al.* also gives reasonable agreement with the data.

D. Results for ^{90}Zr

Before our measurements on ^{90}Zr, no reaction cross-section data above 99 MeV existed, and the new results indicate larger reaction cross sections and a different slope than what earlier data at 40–60 MeV suggest. The global potential by Cooper *et al.* agrees well with our results as does the prediction by Koning and Delaroche, but the two calculations give different slopes. The microscopic calculation by Amos *et al.* somewhat underestimates our reaction cross sections.

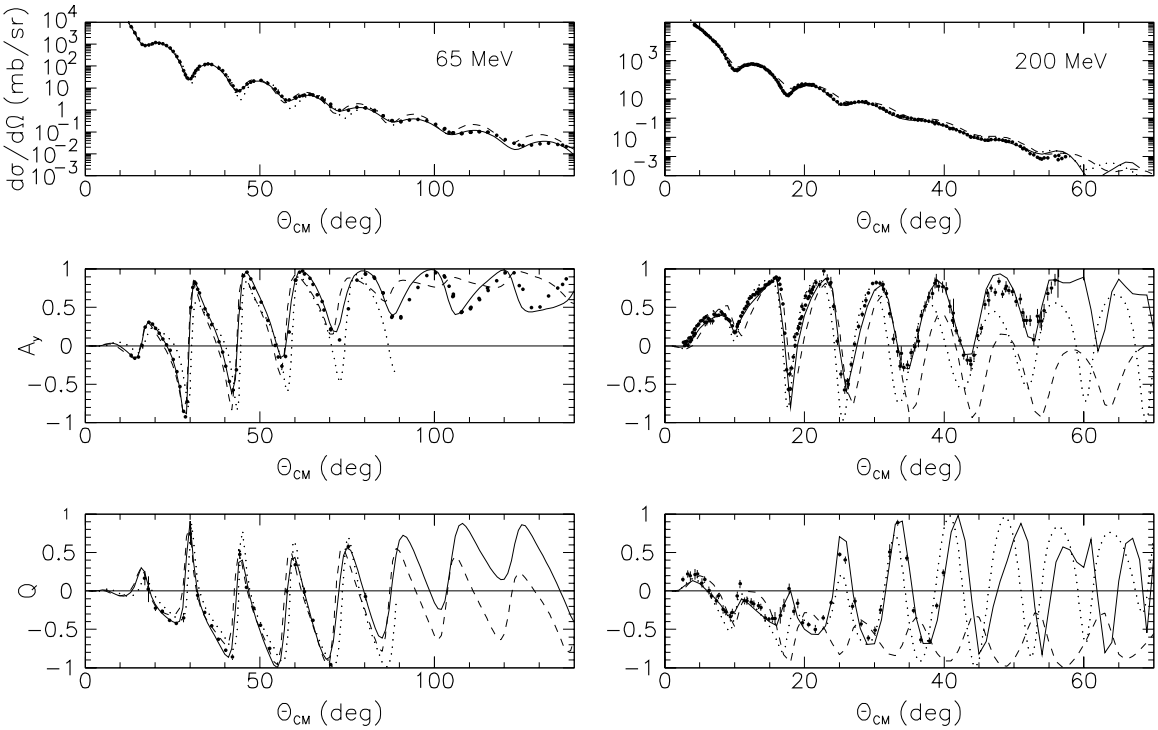

FIG. 10. Angular distributions for the elastic scattering of 65 and 200 MeV protons from ^{208}Pb. See text and Fig. 5 caption for details of the theoretical calculations. Experimental results are from [21,22].

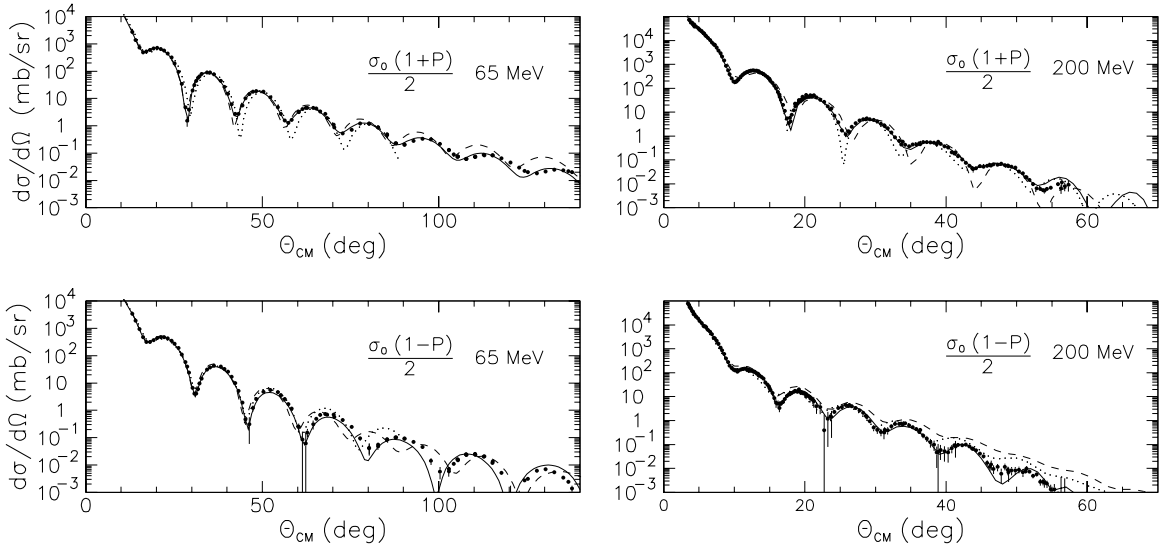

FIG. 11. Angular distributions for σ_+ and σ_- in the elastic scattering of 65 and 200 MeV protons from ^{208}Pb. See text and Fig. 5 caption for details of the theoretical calculations.

E. Results for ^{208}Pb

For ^{208}Pb, one can immediately observe that the earlier inconsistencies for the reaction cross section between experimental results and theoretical predictions have been clarified by our new data; and, as in the case for ^{12}C, some of the earlier measurements can be brought into question. Although the results of Cooper *et al*. indicate systematically higher reaction cross sections than the other two predictions, all three predictions agree fairly well with our measurements. The angular distributions for the differential cross sections, asymmetries, and spin rotations [21,22] are shown in Fig. 10, and those for σ_+ and σ_- in Fig. 11. All angular distributions are well reproduced by all approaches. Also note that the quality of the calculations is very much the same for σ_+ and σ_- for this nucleus.

V. SUMMARY AND CONCLUSION

Proton reaction cross sections have been measured on ^{12}C, ^{40}Ca, ^{90}Zr, and ^{208}Pb at six energies in the range 80–180 MeV and for ^{58}Ni at one energy. The experimental method was based on a modified transmission technique.

Prior to this work, the quality of reaction cross section data was clearly much better below 50 and above 200 MeV. The new data on these four targets improve the situation considerably, especially for ^{208}Pb, where the theoretical predictions were considerably larger than the older experimental values. Our new reaction cross-section values appear to be internally consistent; in addition, they are reproduced quite well by predictions with microscopically as well as macroscopically derived potentials.

We performed several calculations with two global potentials, demonstrating the difficulties in simultaneously reproducing reaction cross-section data and angular distributions for differential cross sections, asymmetries, and spin-rotation parameters. Our calculations have also shown that potentials derived by the Dirac formalism are as successful as those based on the traditional nonrelativistic parametrizations at low energies.

We hope that our data, in combination with earlier experimental results on angular distributions, will stimulate the search for more reliable global potentials.

ACKNOWLEDGMENTS

This project has been financed within the Swedish-South African (SIDA/NRF) partnership program under Grant Number SWE-SRP-2000–001, and by the South African National Research Foundation under Grant Number GUN2053773. We also thank colleagues at KVI Groningen, IUCF Bloomington, and TSL Uppsala for providing targets for our experimental program. We thank the Melbourne group (Ken Amos, Pradip Deb, and Steve Karataglidis) for providing us with numerical values of their calculations.

[1] M. Lantz, M. N. Jacobs, A. Auce, R. F. Carlson, A. A. Cowley, S. V. Förtsch, G. C. Hillhouse, A. Ingemarsson, R. Johansson, K. J. Lawrie, M. J. Shachno, F. D. Smit, J. A. Stander, G. F. Steyn, G. Tibell, and J. J. van Zyl, in *Proceedings International Conference on Nuclear Data for Science and Technology*, AIP Conf. Proc. No. 769, edited by R. C. Haight *et al*. (AIP, New York, 2005), p. 846.

[2] A. Ingemarsson, G. J. Arendse, A. Auce, R. F. Carlson, A. A. Cowley, A. J. Cox, S. V. Förtsch, R. Johansson, B. R. Karlson, M. Lantz, J. Peavy, J. A. Stander, G. F. Steyn, and G. Tibell, Nucl. Phys. **A696**, 3 (2001).

[3] A. Ingemarsson, J. Nyberg, P. U. Renberg, O. Sundberg, R. F. Carlson, A. J. Cox, A. Auce, R. Johansson, G. Tibell, Dao T. Khoa, and R. E. Warner, Nucl. Phys. **A676**, 3 (2000).

[4] A. Ingemarsson, J. Nyberg, P. U. Renberg, O. Sundberg, R. F. Carlson, A. Auce, R. Johansson, G. Tibell, B. C. Clark, L. Kurth Kerr, and S. Hama, Nucl. Phys. **A653**, 341 (1999).
[5] H. Fujita, Y. Fujita, G. P. A. Berg, A. D. Bacher, C. C. Foster, K. Hara, K. Hatanaka, T. Kawabata, T. Noro, H. Sakaguchi, Y. Shimbara, T. Shinada, E. J. Stephenson, H. Ueno, and M. Yosoi, Nucl. Instrum. Methods A **484**, 17 (2002).
[6] R. F. Carlson, W. F. McGill, T. H. Short, J. M. Cameron, J. R. Richardson, W. T. H. van Oers, J. W. Verba, P. Doherty, and D. J. Margaziotis, Nucl. Instrum. Methods **123**, 509 (1975).
[7] A. Auce, R. F. Carlson, A. J. Cox, A. Ingemarsson, R. Johansson, P. U. Renberg, O. Sundberg, and G. Tibell, Phys. Rev. C **53**, 2919 (1996).
[8] R. F. Carlson, At. Data Nucl. Data Tables **63**, 93 (1996).
[9] E. D. Cooper, S. Hama, B. C. Clark, and R. L. Mercer, Phys. Rev. C **47**, 297 (1993).
[10] A. J. Koning and J. P. Delaroche, Nucl. Phys. **A713**, 231 (2003).
[11] K. Amos, S. Karataglidis, and P. K. Deb, Phys. Rev. C **65**, 064618 (2002).
[12] J. Klug, J. Blomgren, A. Ataç, B. Bergenwall, A. Hildebrand, C. Johansson, P. Mermod, L. Nilsson, S. Pomp, U. Tippawan, K. Elmgren, N. Olsson, O. Jonsson, A. V. Prokofiev, P.-U. Renberg, P. Nadel-Turonski, S. Dangtip, P. Phansuke, M. Österlund, C. Le Brun, J. F. Lecolley, F. R. Lecolley, M. Louvel, N. Marie-Noury, C. Schweitzer, Ph. Eudes, F. Haddad, C. Lebrun, A. J. Koning, and X. Ledoux, Phys. Rev. C **68**, 064605 (2003).
[13] A. Ingemarsson and M. Lantz, Phys. Rev. C **67**, 064605 (2003).
[14] A. Ingemarsson and M. Lantz, Report TSL/ISV-2005-0286, http://www4.tsl.uu.se/tsl/tsl/Rapporter.
[15] G. Fäldt, A. Ingemarsson, and J. Mahalanabis, Phys. Rev. C **46**, 1974 (1992).
[16] H. O. Meyer, P. Schwandt, G. L. Moake, and P. P. Singh, Phys. Rev. C **23**, 616 (1981).
[17] H. Sakaguchi, M. Yosio, M. Nakamura, T. Noro, H. Sakamoto, T. Ichihara, M. Ieiri, Y. Rakeuchi, H. Togawa, T. Tsutsumi, H. Ikegami, and S. Kobayashi, in *Proceedings of the Sixth International Symposium on Polarization Phenomena in Nuclear Physics*, Osaka, 1985, edited by M. Kondo, S. Kobayashi, M. Tanifuji, T. Yamazaki, K.-I. Kubo, and N. Onishi, J. Phys. Soc. Jpn. Suppl. **55**, 61 (1986).
[18] A. Ingemarsson, T. Johansson, and G. Tibell, Nucl. Phys. **A322**, 285 (1979).
[19] H. O. Meyer, P. Schwandt, W. W. Jacobs, and J. R. Hall, Phys. Rev. C **27**, 459 (1983).
[20] Z. Yu, R. E. Segel, T.-Y. Tung, R. D. Bent, C. C. Foster, J. Goodwin, G. Hardie, and J. Homolka, Phys. Rev. C **53**, 1725 (1996).
[21] H. Sakaguchi, M. Nakamura, K. Hatanaka, A. Goto, T. Noro, F. Ohtani, H. Sakamoto, H. Ogawa, and S. Kobayashi, Phys. Rev. C **26**, 944 (1982).
[22] D. A. Hutcheon, W. C. Olsen, H. S. Sherif, R. Dymarz, J. M. Cameron, J. Johansson, P. Kitching, P. R. Liljestrand, W. J. McDonald, C. A. Miller, G. C. Neilson, and D. M. Sheppard, Nucl. Phys. **A483**, 429 (1988).